Ga_2Se_3 nanowires via Au-assisted heterovalent exchange reaction on GaAs

Federico Berto,[#,%,¥] *Niloofar Haghighian,*[#,†] *Katja Ferfolja,*[&] *Sandra Gardonio,*[&] *Mattia Fanetti,*[&] *Faustino Martelli,*[$] *Valentina Mussi,*[$] *Vladimir G. Dubrovskii,*[¶] *Igor V. Shtrom*[§], *Alfonso Franciosi*[#, %] *and Silvia Rubini*[#*]

Istituto Officina dei Materiali, Consiglio Nazionale delle Ricerche, Trieste, Italy

% Dipartimento di Fisica, Università di Trieste, Trieste, Italy

& University of Nova Gorica, Nova Gorica, Slovenia

$ Istituto per la Microelettronica e Microsistemi, Consiglio Nazionale delle Ricerche, Roma, Italy

¶ ITMO University, Kronverkskiy pr. 49, 197101 St. Petersburg, Russia

§ St. Petersburg State University, Universitetskaya Emb. 13B, 199034, St. Petersburg, Russia

Contact: rubini@iom.cnr.it

ABSTRACT

Out-of-plane Ga_2Se_3 nanowires are grown by molecular beam epitaxy via Au-assisted heterovalent exchange reaction on GaAs substrates in the absence of Ga deposition. It is shown that at a suitable temperature around 560°C, the Au-decorated GaAs substrate releases Ga atoms, which react with the incoming Se and feed the nanowire growth. The nanowire composition, crystal structure and morphology are characterized by Raman spectroscopy and electron microscopy. The growth mechanism is investigated by x-ray photoelectron spectroscopy. We explore the growth parameter window and find an interesting effect of shortening the nanowires after a certain maximum length. The nanowire growth is described within a diffusion transport model, which explains the non-monotonic behavior of the nanowire length versus the growth parameters. Nanowire shortening is explained by the blocking of Ga supply from the GaAs substrate by thick, in-plane worm-like Ga_2Se_3 structures, which grow concomitantly with the nanowires, followed by backward diffusion of Ga atoms from the nanowires down to the substrate surface.

INTRODUCTION

Ga_2Se_3 belongs to the III_2-VI_3 family of materials. These chalcogenides are characterized by intrinsically defective structures, with cation vacancies originating from the competition between the tetrahedral bonding typical of III-V and II-VI compounds, and the presence of an extra electron per anion-cation pair [1]. Ga_2Se_3 crystallizes in a defective zincblende structure, where one third of the Ga sites are vacant [2, 3]. The vacancies can be randomly distributed (α-phase)

or ordered (β-phase), resulting in superstructures with different symmetries (orthorhombic or monoclinic) [2-7] depending on the growth conditions.

Optical and electronic properties of Ga_2Se_3 have been widely investigated in the past, especially due to its role as interface material at III-V/II-VI junctions [8-10] and to peculiar optical anisotropies related to the vacancy ordering [11]. The potential of Ga_2Se_3 as the negative electrode material for Li batteries has recently been evaluated [14]. Ga_2Se_3 has also been proposed as a possible photocatalyst for water splitting under visible light [15]. Furthermore, if doped with selected magnetic impurities, it becomes a promising diluted magnetic semiconductor. For example, room temperature ferromagnetism has been observed in Cr-doped Ga_2Se_3 [16].

Epitaxial β-Ga_2Se_3 layers have been grown by molecular beam epitaxy (MBE) on III-V [17, 18, 6] and Si [7, 1] substrates with different symmetries of the vacancy ordering depending on the substrate (see, for example, Ref. [6] and references therein). It has been shown that GaAs strongly reacts with Se hydrides, leading to the formation of Ga_2Se_3 layers in the absence of any external Ga supply [10, 19]. A heterovalent exchange reaction between group V and VI elements, activated at high enough temperatures, was invoked to describe the growth mechanism. Formation of α- or β-phase was found to depend on the substrate temperature. A similar process was more recently reported involving GaSb, where Ga_2Se_3 material was obtained by exposing GaSb to a Se flux at high temperature, and then used as a buffer layer for epitaxial growth of Bi_2Se_3 by MBE [20]. Such a growth led to the formation of voids in the GaSb substrate, with the Ga_2Se_3 film being partially suspended and supported only by a few GaSb nanopillars [20].

No information can be found in the literature on Ga_2Se_3 in the form of freestanding nanowires (NWs), while a few examples of In based III_2-VI_3 NWs are known. In_2Te_3 NWs were synthesized by Au-assisted VLS mechanism [21, 22, 23]. The nanostructure properties were investigated, highlighting their performance as photodetectors in single NW devices [22]. In_2S_3 nanocrystals with high aspect ratio were grown in the form columnar microcrystals by thermal evaporation without the use of a catalyst [24]. Finally, In_2Se_3 NWs were synthesized by the Au-assisted vapor-liquid-solid (VLS) mechanism by several groups [25, 26, 27, 28]. High quality nanostructures were obtained and investigated as possible Li-storage materials because of the intrinsic presence of structural vacancies [29], and as a potential material system for high-performance visible light photodetectors [27] and field emitters [28]. Similar structural vacancies are also intrinsically present in Ga_2Se_3. On the other hand, silicon NWs [30] show excellent performance as Li battery anodes. We can thus envisage the use of Ga_2Se_3 NWs in high performance Li batteries.

Far less reports are available for Ga-based III_2-VI_3 nanostructures. Highly ordered horizontal Ga_2S_3 NWs were recently obtained by chemical vapor deposition on sapphire [31]. One-dimensional horizontal growth was driven by Au particles in a VLS mechanism and was favored over vertical growth due to the high growth temperature and low precursor fluxes. The nanostructures showed excellent nonlinear optical properties. Finally, single crystalline Ga_2S_3 nanotubes were obtained by conversion of GaAs NWs exposed to sulphur vapor [32]. The conversion process was investigated as a function of the exposure time. It was found to proceed via the formation of epitaxial core-shell GaAs-Ga_2S_3 NWs, followed by the development of hollow Ga_2S_3 tubes. The tubes formed by retraction of GaAs cores due to injection and coalescence of vacancies into the Kirkendall voids, with simultaneous evaporation of As [32].

In this paper, we demonstrate that freestanding Ga_2Se_3 NWs can be obtained by MBE on Au-decorated GaAs surfaces without any external Ga supply, via a heterovalent exchange reaction mediated by Au nanoparticles. We show that at a suitable temperature, the presence of Au on the surface favors the decomposition of the GaAs substrate and the release of Ga atoms, which react with the incoming Se and feed the NW growth. We explore the growth parameter window and find that the NWs start to shorten after a certain maximum length. The NW composition, crystal structure and morphology are characterized by Raman spectroscopy and electron microscopy. The growth mechanism is investigated by x-ray photoelectron spectroscopy (XPS). The NW growth is described within a kinetic model, which explains the peculiar non-monotonic behavior of the NW length versus the growth parameters.

METHODS

Ga_2Se_3 NWs were grown on epi-ready n-type Si-doped GaAs (100) substrates in a multi-chamber ultrahigh vacuum system including an MBE growth chamber equipped with Se and Bi effusion cells, a metallization chamber for thermal evaporation of Au and an analysis chamber for XPS. After thermal desorption of the surface oxide layer, the substrates were transferred into the metallization chamber where 1 nm of Au was deposited at room temperature. Following 15 min annealing at 600°C for thermal dewetting of the Au layer, the substrate was exposed to Se flux. In seldom cases, Bi flux was used together with Se, but no noticeable differences were found between the samples grown with or without Bi flux, and in the following we will not specify that (more information is given in the Supporting Information (SI) 1). Beam equivalent pressures (BEPs) of Se between 1×10^{-6} and 4×10^{-6} Torr were explored. The corresponding Se fluxes were measured by an ion gauge located at the substrate.

The NW morphology was investigated by scanning electron microscopy (SEM), using a field-emission SEM Zeiss SUPRA 40 operated at 10 keV, with a nominal point resolution of 1.5 nm. Lengths and diameters of more than 40 NWs were measured for each sample. Structural characterization was performed in a field-emission transmission electron microscope (TEM) Jeol JEM2100F-UHR operated at 200 KeV. The material composition was investigated by energy-dispersive X-ray spectroscopy (EDX) in both SEM and TEM. For EDX in SEM, we used a JEOL JSM 7100 SEM equipped with a X-Max80 EDX (Oxford Instruments). For STEM/EDX analysis, the same TEM was used in scanning TEM (STEM) mode at 200 kV. STEM images were acquired with an annular dark-field detector. EDX analyses were performed with X-Max80T (Oxford Instruments).

Raman spectra were acquired in a DXR2xi Thermo Fisher Scientific Raman Imaging Microscope with laser excitation at 532 nm.

At selected stages of NW growth, XPS analysis was performed in an Al-Kα photoemission chamber (Surface Science Instrument) connected to the MBE system, with an overall energy resolution of 0.1 eV.

RESULTS

Ga_2Se_3 NWs were obtained by exposing the GaAs (100) surface decorated with Au nanoparticles (NPs) to a Se flux. Figure 1 shows plan-view SEM images of the samples grown for 15 min with a Se BEP of 4×10^{-6} Torr at substrate temperatures between 480°C and 600°C. Within this temperature window, a percentage of thin and straight NWs is found with the projection aligned to the <001> directions of the substrate surface. Careful analysis of the SEM

images shows that the NW growth direction makes an angle of 45° with the substrate plane, indicating that they grow along the <110> directions of the GaAs substrate. The analysis of NW orientation with respect to the substrate is detailed in SI 2. In the following, the NW length quoted on the left of each graphics corresponds to the measured NW projection onto the (001) substrate surface. We report on the right scale the real NW length as calculated considering the angle they make with the substrate. Considering that in several cases we observe in the same NW sample a wide majority of NWs with length concentrated in a relatively narrow range of values,

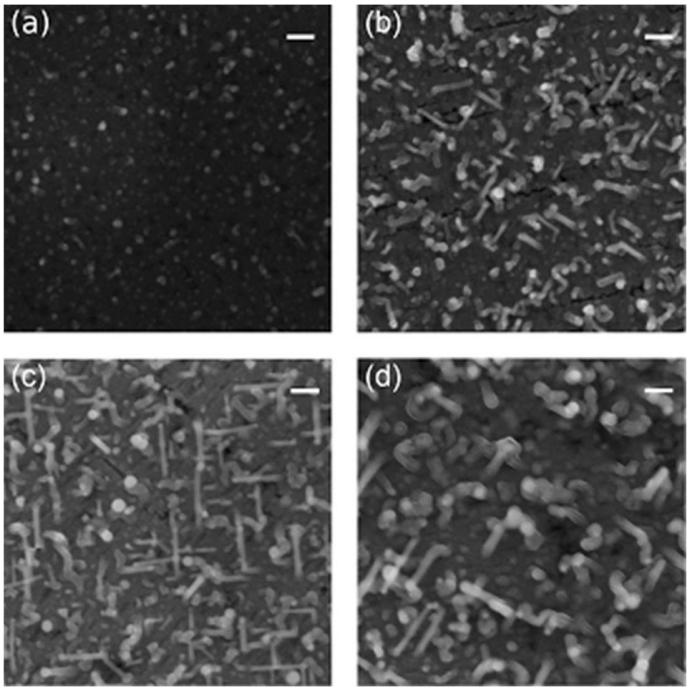

Figure 1. Plan-view SEM images of Ga_2Se_3 NW samples grown for 15 min under a Se BEP of 4×10^{-6} Torr at different substrate temperatures: (a) 480°C, (b) 520°C, (c) 560°C, and (d) 580°C. Scale bars correspond to 100 nm.

and few nanowires with length quite far from the average value, in order to maximize the information for the reader we report the data in the form of box plot: the extremes of each box

correspond to the 25th and 75th percentile of the length distribution, respectively, the mark in the center to the median, while the whiskers span the entire range of the measured values.

The NWs can continue growing after the initial nucleation step only at high enough substrate temperatures. This is clearly seen from Fig. 2 (a), where the NW length after 15 and 60 min of growth is shown as a function of temperature. We will therefore focus on the samples grown at 560°C, with the longest Ga_2Se_3 NWs. A representative plan view of the sample after 30 min of growth is shown in Fig. 2 (b). Together with the NWs, some thicker, worm-like structures are also observed, most of which do not grow away from the substrate, but rather develop along the substrate surface. Both NWs and worm-like structures exhibit Au NPs at the top, as can be observed in Fig. 2(b) where the NPs are indicated by arrows. The NPs found at the top of the out-of-plane NWs are smaller and more uniform in size compared with those observed on the worm-like structures. This is illustrated in the histogram in Fig. 2 (c) where the statistics for a sample grown for 30' with a Se BEP of 4 ×10-6 Torr is shown. The diameter of the Au NPs seems therefore to be a decisive factor in determining the formation of out-of-plane NWs or in-plane worm-like structures. More information about the size dependence of the nanostructure morphology can be found in SI 3.

The NW diameter was found to be in the range of 20-30 nm independently of growth time and Se BEP, SEM images of representative samples grown for different time and with different Se BEP are shown in SI 4. Kinks were occasionally observed along the NW axis, as indicated by the white arrow in Fig. 2(b).

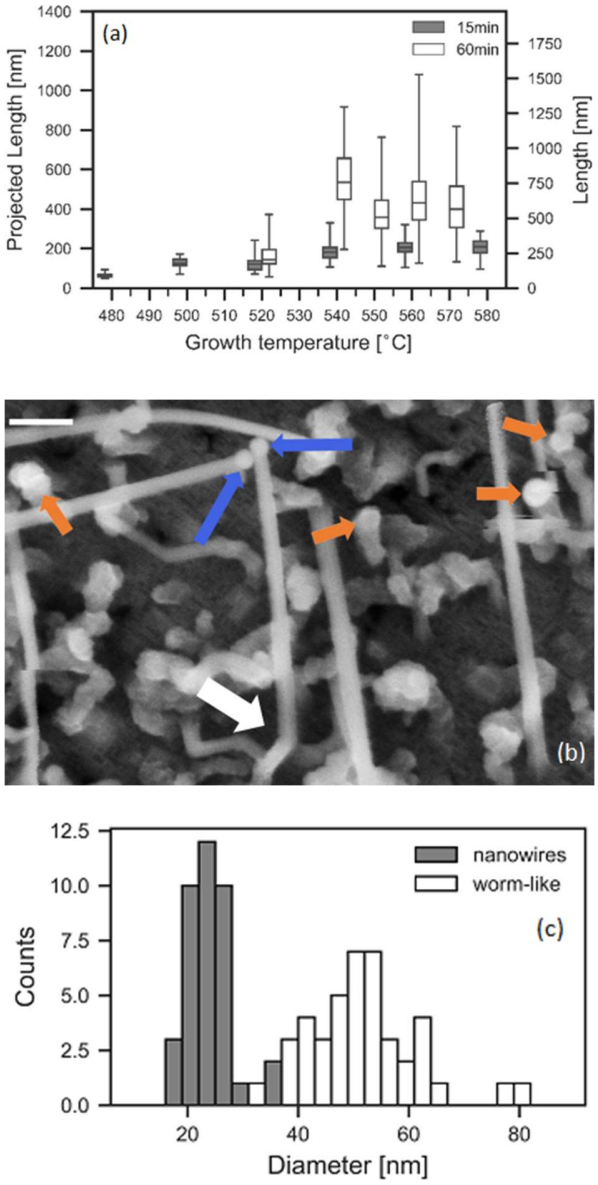

Figure 2. (a) Ga_2Se_3 NW lengths measured after 15 min (grey boxes) and 60 min (white boxes) growth times at a fixed Se BEP of 4×10^{-6} and different substrate temperatures. (b) Plan view SEM image of sample grown for 30 min with a Se BEP of 4×10-6 Torr at 560°C: Au nanoparticles at the tip of NWs and worms-like structures are indicated with blue/long and orange/short arrows, respectively. A kinked NW is indicated by a white arrow. Scale bar corresponds to 100 nm. (c) Diameter distributions of NWs and worm-like structures, obtained from statistical analysis of the sample grown for 30 min with a Se BEP of 4×10^{-6} Torr at 560°C.

Figure 3 shows the dependence of the NW length on the growth time for different Se BEPs. In all cases, the NW length first increases almost linearly with time, then saturates at a maximum value and eventually decreases for longer times.

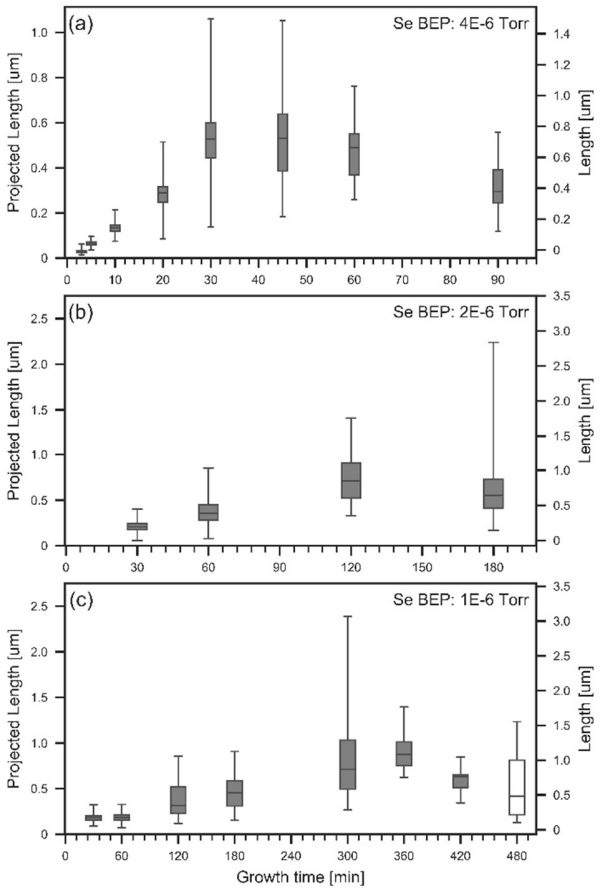

Figure 3. Ga_2Se_3 NW length versus the growth time at a substrate temperature of 560°C and three different Se BEP: (a) 4×10^{-6} Torr, (b) 2×10^{-6} Torr, and (c) 1×10^{-6} Torr. The point at 480 min in panel (c) displayed as white box, corresponds to a 360 min growth followed by 120 min annealing without Se flux, for a total time of 480 min at growth temperature.

This is a quite uncommon behavior whose presence is independent of the Se flux. This feature is pointed out in particular in Fig. 3(c) where you can see a white point placed at 480 min. The related NWs have been actually grown for 360 min and then exposed to a thermal annealing at

the same growth temperature of 560 °C for further 120 min in the absence of a Se flux. As you can notice, the NW length has decreased in those 120 minutes more than that of the wire continuously grown for 420 min. This feature is a clear indication that the shortening of the NWs after having reached a maximum length, is a process completely independent of the Se flux: it occurs both in presence of a Se flux, whatever its amount, and in the absence of it.

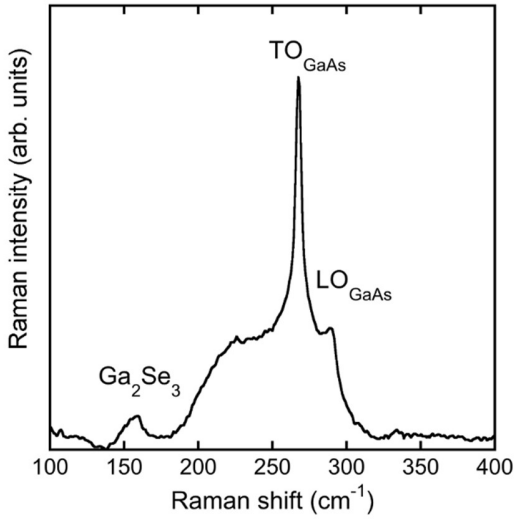

Figure 4. Raman spectrum of a NW sample under 532 nm excitation. The sharp signal at 155 cm^{-1} is characteristic of Ga_2Se_3.

Several characterizations performed on the NWs confirmed that they are composed of Ga_2Se_3. Unpolarized Raman spectra were acquired on the as grown samples, therefore including both the standing NWS and the wormlike structures. A typical spectrum observed is shown in Fig. 4, for a sample grown for 30 min with a Se BEP of 4×10^{-6} Torr. We observe a sharp peak at 155 cm^{-1}, which is a clear signature of the presence of Ga_2Se_3 [2, 19]. The typical GaAs TO and LO phonon scattering signals at 267 cm^{-1} and 292 cm^{-1}, respectively, originate from the GaAs substrate. The broad shoulder at the intermediate energies is due to unresolved contributions

from several lines of Ga_2Se_3. Broadening of the Raman peaks is likely due to the presence of structural defects in Ga_2Se_3 [33].

In Fig. 5 we report a SEM image and EDX compositional analysis of a bundle of NWs removed from the substrate and supported by a TEM copper grid. In the low resolution image we can still recognize the NW bodies and the spherical NPs at the tips. The EDS data indicate the

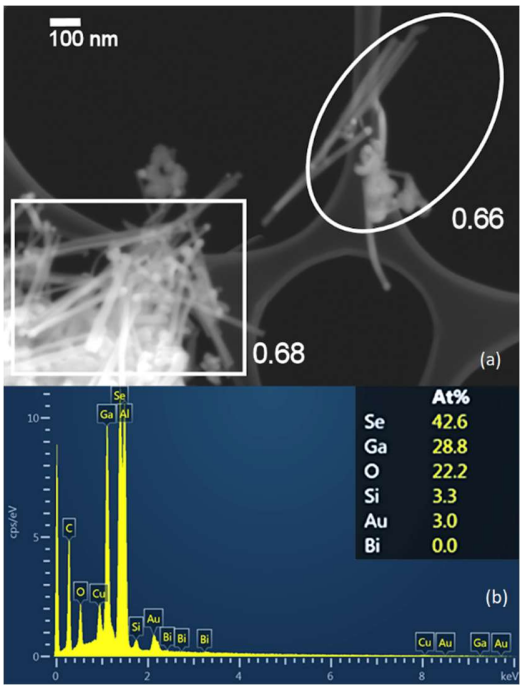

Figure 5. (a) SEM image of a bundle of NWs transferred from the substrate to a TEM copper grid. Scale bar corresponds to 1 µm. The evaluated Ga/Se ratio is indicated beside the boxes. (b) EDS spectrum acquired in the region boxed in (a).

presence of Ga, Se and Au. Al and Cu come from the mounting stage and the TEM grid, respectively. The relative abundance of Ga and Se is 0.68, very close to the nominal 2:3 ratio.

STEM/EDX analysis of single NW samples confirmed that the NW body is composed only of Ga and Se, with Au (and Bi if used during growth) below the detection limit. A representative analysis is shown in Fig. 6. STEM/EDX analysis on single wire does not allow us to precisely

address the Ga:Se NW stoichiometry. In fact, Ga and Se intensities are strongly affected by channeling effects that are particularly strong when NWs are imaged in direction perpendicular to the growth axes [33]. EDX measurements of the NPs resting at the NW tip reveal that it is composed of Au and Ga, with Ga concentration around 5 atomic %. A weak Se signal from the NPs is also detected, around 1%. The worm-like structures are also composed of Ga and Se (see SI 3 for more details). TEM analysis of representative single NWs showed the NPs at the NW tip are 10-40% larger than the NW diameter.

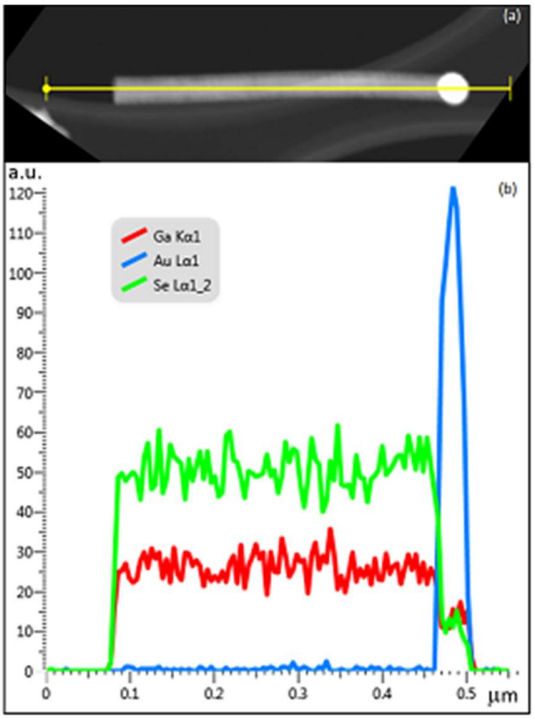

Figure 6. (a) Dark-field STEM image and (b) EDX line scan of a representative Ga_2Se_3 NW.

High-resolution (HR) TEM study reveals that both NWs and worm-like structures are crystalline. Unfortunately, more accurate analysis of the structure by electron diffraction along the NW zone axes was hindered by fast degradation of the NWs under the electron beam. Still, in several cases, a structure equivalent to the one reported in Ref. [6] is observed. In Fig. 7 we show

two representative wires, one of them kinked, as occasionally observed (see for instance Fig. 2(b)). In the absence of selected area diffraction images, we analyzed the Fast Fourier Transformation (FFT) of the high resolution images. As illustrated in Fig. 7, the most frequently observed periodicities are 1.9 Å, 2.7 Å and 3.1 Å , which correspond to the <220>, <200> and <111> directions of α-Ga_2Se_3, respectively [3]. The wires appear to be characterized by a high density of stacking faults on the two sets of {111} planes. Most of the stacking faults stop at the intersection of both {111} planes. These features were observed in Ga_2Se_3 epitaxially grown on GaAs [6], and associated to the ordering of the Ga vacancies on the {111} planes of the α-Ga_2Se_3, leading to the monoclinic β-Ga_2Se_3 structure described in Ref [2].

Many of the observed wires grow in the <110> direction, as the one in Fig. 7(a-c). In this case the wires are in epitaxial relation with the GaAs substrate, with the <100> directions of the defective zincblende α-phase Ga_2Se_3 and of the GaAs substrate aligned with each other. No direct information could be drawn from the FFT about the presence or absence of any ordered superstructures. However, the high density of stacking faults along the {111} planes suggests that ordering of the vacancies characterizing the β-phase is present [6].

The NP at the NW top has a nearly spherical shape, and the interface with the NW is neither flat nor perpendicular to the growth axis, which may suggest a vapor-solid-solid (VSS) growth mechanism [35] or be due to a NP reconfiguration during the cooling down process. Some NWs are kinked due to a change of their growth direction, as shown in Fig. 7 (d).

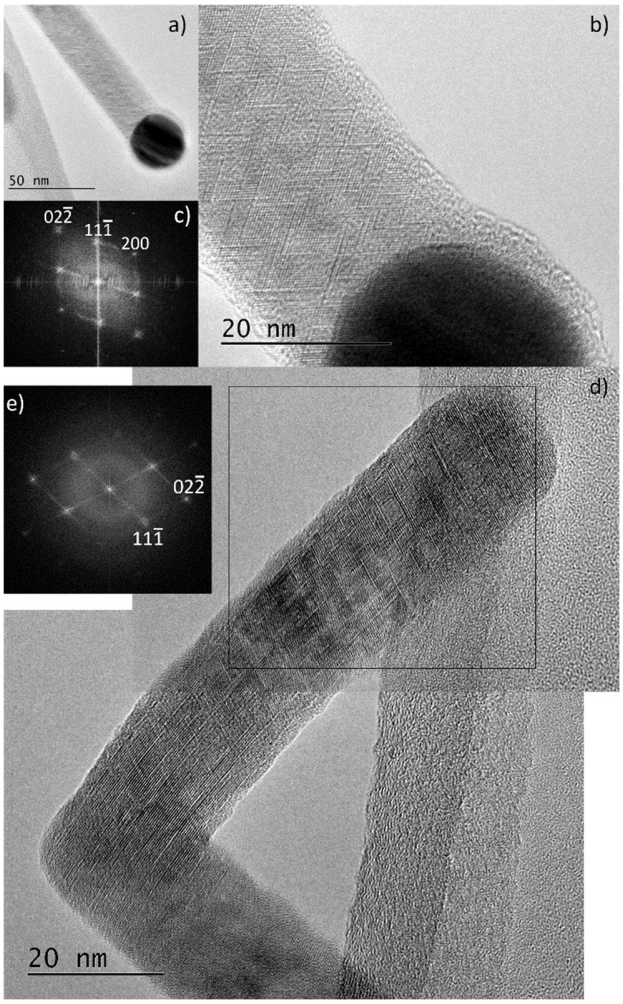

Figure 7. (a) TEM image of a straight NW. (b) HR-TEM image of the same NW. (c) Fast Fourier transform (FFT) of the image from the NW body. (d) HR-TEM of a kinked NW. (e) FFT of the image from the boxed region in (d).

XPS spectra were acquired at selected stages of growth under a Se BEP of 4×10^{-6} Torr. Figure 8 shows that, after annealing at 600°C, the Au $4f_{7/2}$ emission shifts from 84.00 eV typical of pure Au, to 85.54 eV. This reflects the well-known alloying process with Ga, with a Ga content of 67% or higher [36]. When the NW growth starts, the shift is reduced and the Au $4f_{7/2}$ line is detected at 84.7 eV. This shift corresponds to an Au-Ga alloy with 33% Ga and does not much

change with the growth time until the Au line becomes invisible. Due to the surface sensitivity of the XPS measurements, the measured concentration corresponds to Ga content in ~ 2 nm thick surface layer of the NPs, while the EDX data presented above reveal only 5% Ga content in the whole NP. After 45 min of Se deposition, the Au line is barely visible (Fig. 8 (d)), and becomes undetectable after 60 min.

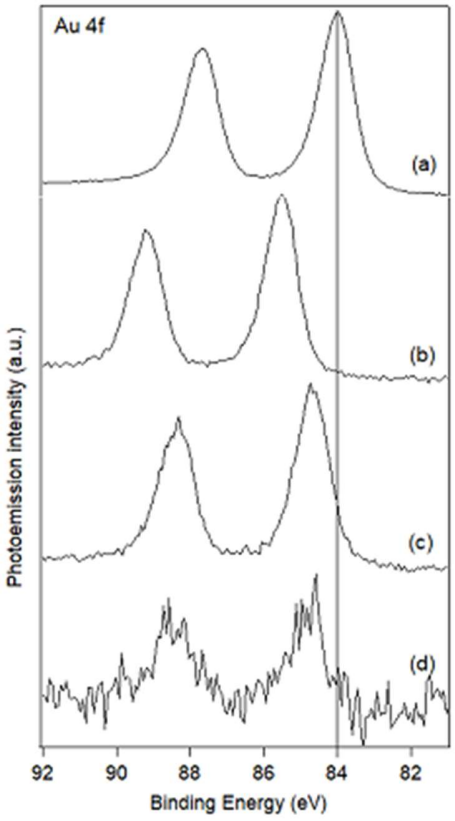

Figure 8. Au 4f core level emission at selected stages of a NW growth experiment: (a) after 1 nm Au deposition on GaAs at room temperature, (b) after annealing at 600°C, (c) after 2 min of Se deposition, and (d) after 45 min of Se deposition. The vertical line indicates the $4f_{7/2}$ binding energy in pure Au (84.0 eV according to Ref. [37]).

The As 3d and Ga 3d emissions at different stages of the growth process are shown in Fig. 9. The As 3d line is fitted by a spin-orbit doublet [38], shown by the dashed blue lines, and the

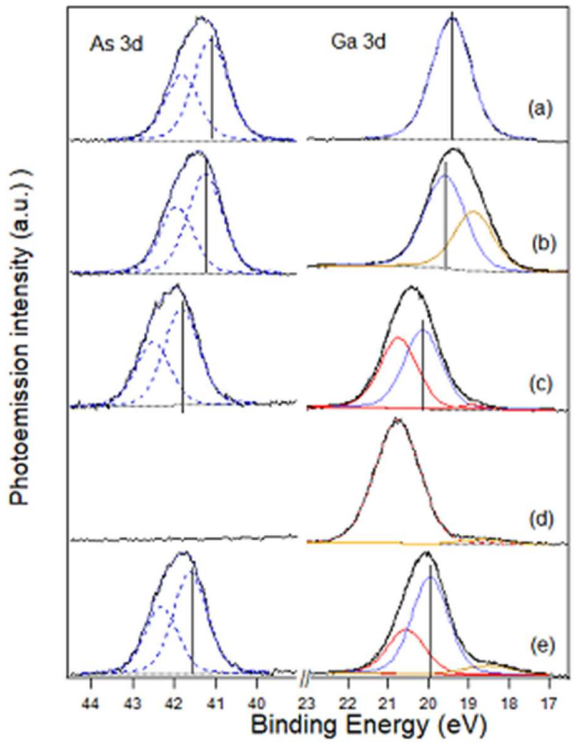

Figure 9. As 3d (left panels) and Ga 3d (right panels) XPS spectra at different stages of the growth process. (a) Clean GaAs surface; (b) after deposition of 1 nm Au and 15 min annealing at 600°C; (c) after 3 min exposure to Se flux; (d) after 45 min exposure to Se flux. For comparison, we also show spectra obtained after exposing the GaAs surface to Se flux for 45 min in the absence of Au in (e). The dashed blue lines show the deconvolution of the As 3d peak into the spin-orbit doublet. The rightmost vertical lines mark the expected position of the GaAs-related Ga 3d emission as obtained from the observed As 3d position (leftmost vertical line) and the measured energy separation between As 3d and Ga 3d peaks for clean GaAs. The blue line denotes such a GaAs-related component of the Ga 3d lineshape. The yellow and red lines denote Ga 3d contributions shifted to higher and lower binding energies, respectively.

position of the As $3d_{5/2}$ component is marked by a vertical line. The As 3d core level emission does not display any lineshape change throughout the entire growth process, but becomes weaker for longer exposures to Se flux. After 45 minutes of exposure, it is no longer visible [Fig. 9(d)].

We analyze the evolution of the Ga 3d line versus growth time relative to the GaAs-related component (corresponding to the solid blue lines in Figs. 9). The latter is fixed (rightmost vertical line) at the position expected from the observed As 3d position (leftmost vertical line) in each case and the measured energy separation between the As $3d_{5/2}$ feature and the Ga 3d peak for clean GaAs (21.67 eV in Fig. 9 (a)). After the Au deposition and annealing at 600°C [Fig. 9(b)], we detect the appearance of a component at higher binding energy, shown by the yellow line. This emission should correspond to metallic Ga alloyed with Au. Upon exposure to Se flux, a third component appears at a lower binding energy, shown by the red line in Fig 9 (c). This component becomes dominant for longer deposition times and is related to the Ga-Se reaction. After 45 min of exposure to the Se flux, the GaAs-related component is no longer visible, as shown in Fig. 9 (d). A low energy peak is still visible, at an energy close to that of metallic Ga [39].

Figures 10 (a) and (b) show the Se 3d core level emission observed from the Au-decorated GaAs surface after exposure to a Se flux for 2 min and 45 min, respectively. As soon as detected, the Se 3d spectrum appears to be composed of two spin-orbit doublets. The observed lineshape is compellingly similar to that reported for β-Ga_2Se_3, where the two doublets correspond to the two inequivalent Se sites in the lattice [1, 5, 8]. The separation between the two doublets is close to 1 eV. The separation between the Se 3d main peak and the high binding energy peak of Ga 3d is 34.55 eV. This value is in good agreement with reported data for Ga_2Se_3, for example 34.65 eV and 34.73 eV for Ga_2Se_3 grown by MBE on Si [1] and GaAs [8], respectively, and 34.66 eV for

selenized GaAs (100) [8]. The observed intensity ratio of the two peaks in Fig. 10 is 0.43, which is close to the expected ratio 1:2 for Se atoms bound to two and three Ga atoms, respectively.

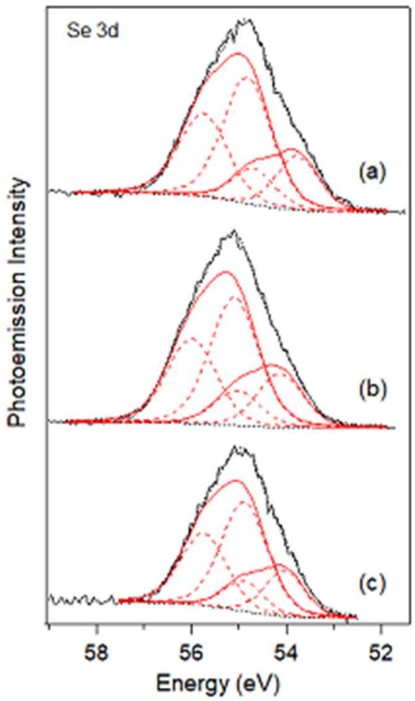

Figure 10. Se 3d core level emission after exposing the GaAs surface with 1 nm of Au annealed at 600°C to Se flux for 2 min (a) and 45 min (b). For comparison we also show the Se 3d emission from GaAs upon exposure to Se flux for 45 min in the absence of Au. The spectra are fitted with the two spin-orbit doublets (red dashed lines), corresponding to the two inequivalent sites of Se. The envelope of each doublet is shown by the red solid lines.

The bottom panels of Figs. 9 and 10 show the Ga 3d, As 3d [Fig. 9(e)], and Se 3d [Fig. 10(c)] core level emissions from the samples grown for 45 min under the same conditions but on clean GaAs without any Au. It is seen that GaAs-related As 3d and Ga 3d emissions are still dominant, while a higher binding energy component appears in the Ga 3d spectrum. The Se 3d emission is

also observed, confirming the selenization of the surface, with the two spin-orbit doublets separated by 0.9 eV. The separation between this peak and the high energy peak of Ga 3d emission equals 34.61 eV, which is in agreement with the literature data for Se-reacted GaAs(100) surface (34.66 eV according to Ref. [8]). The situation remains identical after 60 min of Se deposition (not shown), indicating that a Se-containing layer is present on the surface, but its thickness (on the order of 1 nm) does not increase with exposure time to the Se flux.

Figure 11 shows the cross-sectional morphology and chemical profile of a sample grown for 60 min with a Se BEP of 4×10^{-6} Torr on Au-decorated GaAs (100), compared with a sample exposed for the same time and under the same conditions to the Se flux in the absence of any Au on the substrate. In the sample with Au, we can see some voids penetrating into the substrate, with Au nanoparticles possibly accumulating in the voids. Ga and Se-rich nanostructures are detected on the substrate surface, with thin Ga_2Se_3 NWs growing away from the substrate. No thick Se-rich layer is found on the surface. Therefore, the decrease in the measured NW length at longer growth times is not caused by burying the bottom part of the NWs in a Se-rich layer. This conclusion is confirmed by the data shown in Fig. 3(c), where the NW shortening also takes place during annealing in the absence of a Se flux. No cavities are visible in the cross-sectional SEM image of the sample grown without Au. The substrate surface is flat and contains no detectable Se-rich layer.

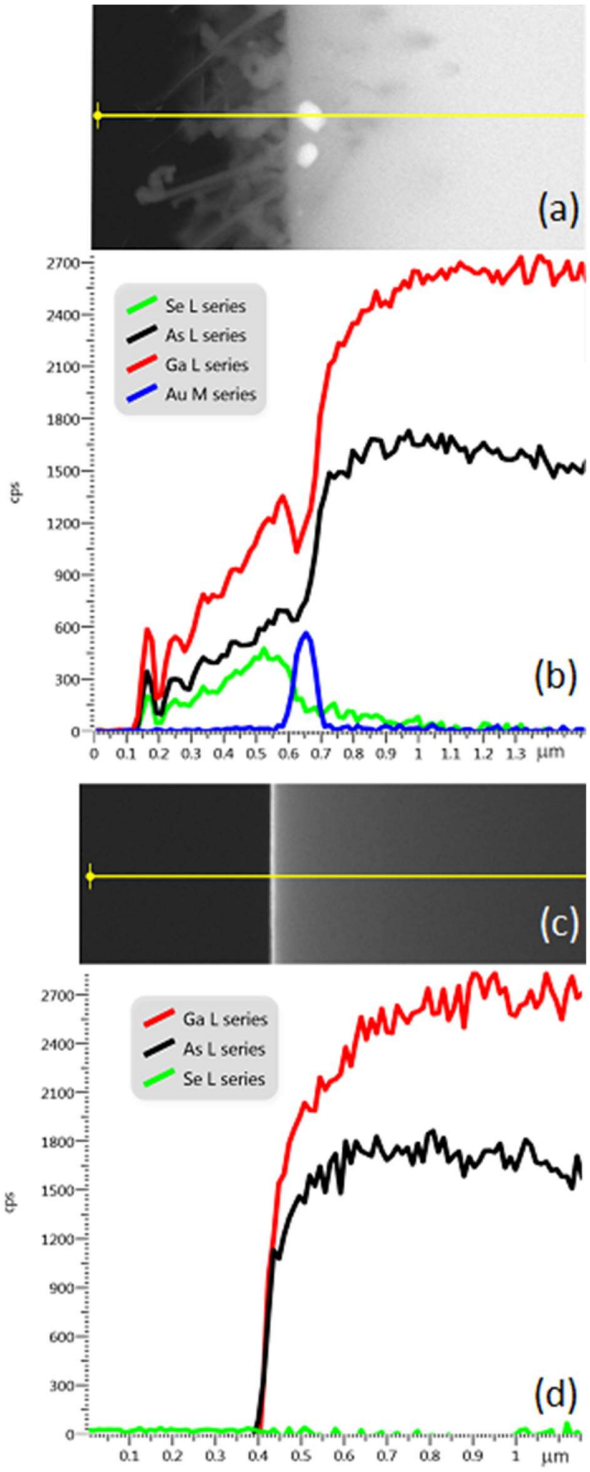
(a)
Se L series
As L series
Ga L series
Au M series
cps
2700
2400
2100
1800
1500
1200
900
600
300
0
0 0.1 0.2 0.3 0.4 0.5 0.6 0.7 0.8 0.9 1 1.1 1.2 1.3 µm
(b)
(c)
Ga L series
As L series
Se L series
cps
2700
2400
2100
1800
1500
1200
900
600
300
0
0.1 0.2 0.3 0.4 0.5 0.6 0.7 0.8 0.9 1 µm
(d)

Figure 11. (a) Cross-sectional SEM image (top panel) and (b) EDX profile (along the line shown in the image) of a NW sample grown for 60 min with a Se BEP of 4×10-6 Torr on Au-decorated GaAs(100) surfaces. (c) Cross-sectional SEM image (top panel) and (d) EDX profile (along the line shown in the image) of a GaAs(100) surface exposed for 60 min to the same Se flux at the same temperature in the absence of any Au nanoparticles.

DISCUSSION

According to the data presented above, our Ga_2Se_3 NWs grow on GaAs (100) without any external Ga flux and only in the presence of Au nanoparticles. Such growth can only occur due to an Au-assisted release of Ga atoms from the GaAs substrate, which subsequently react with the available Se to form Ga_2Se_3. The NW growth should proceed at the tip and be assisted by the nanoparticle consisting of an alloy of Au with the NW material (Ga and Se). We can safely rule out any root growth of NWs because all our experimental data show the presence of a nanoparticle at the NW top as well as at the tip of warm-like parasitic structures. No NW growth occurs without Au. Therefore, the very first NW layer emerges under the nanoparticle and nucleates from the nanoparticle (liquid or solid). This process has a much higher probability compared to catalyst-free nucleation due to a higher degree of supersaturation of Ga_2Se_3 inside the nanoparticle with respect to the rest of the surface. Root growth may occur without the presence of such nanoparticle, but this mechanism may be relevant only for catalyst-free selective area epitaxy, which is not the case of this study. Surface diffusion of Ga from the substrate surface to the droplet is required for NW growth from the nanoparticle in the absence of Ga supply from vapor.

Growth of Ga_2O_3 NWs with no external supply of Ga or O_2 supply was previously achieved via low vacuum thermal treatment of GaAs(100) substrate covered with a thin Au film [40]. Similar with our case, some voids were found in the substrate [41] and the Ga_2O_3 NW formation was explained by the reaction of GaAs with the Au layer, allowing a supply of Ga atoms which bind with the residual oxygen in the growth chamber.

The stability of GaAs in contact with Au was extensively studied in the past in connection with the electrical properties of metal/semiconductor junctions. It is well documented that Ga migrates into Au at temperatures above 400°C, (see, for example, Ref. [42] and references therein). Decomposition of the reacted volume of GaAs releases As, which diffuses through a polycrystalline Au-Ga layer and re-evaporates [43]. The rate of this process can be controlled, for example, by tuning the As_2 pressure in the chamber or using encapsulating layers [42].

On the basis of the experimental evidences depicted above we can outline a phenomenological description of the NW growth process in our system as follows: Au-assisted decomposition of GaAs in the annealing step leads to the formation of binary Au-Ga NPs (with a negligible As content), which is usually liquid at temperatures higher than 400°C depending on the actual Ga content [42]. The formation of Au-Ga alloy is demonstrated by the XPS data in Fig. 8(a,b) and 9(a,b). Subsequent deposition of Se onto Au-Ga NPs promotes the formation of a supersaturated ternary Au-Ga-Se alloy NPs from which the NWs grow. Ga supply comes from the decomposition of the GaAs substrate. Figure 11 clearly demonstrates the presence of voids deep in GaAs substrate decorated with Au, while in the absence of Au and under otherwise identical conditions the surface remains flat upon exposure to the Se flux. Based on the EDX and XPS data, we suggest that Ga alloys with Au, and that this leads to re-evaporation of excess As atoms and explains the formation of voids.

The nanostructure nucleation strictly depends on the presence of the Au nanoparticles that are found at the free end of the NWs and at one extremity of the wormlike structures. Growth is indeed observed only if the GaAs substrate is Au- decorated, either by dewetting of a continuous Au film as in the experiments described above, or through size selected colloidal nanoparticles as in SX. In the absence of Au, neither NWs nor wormlike nanostructures are obtained (See Fig. 11). This strongly support the fact that further growth of Ga_2Se_3 NWs and worm-like structures fed by the Ga supply is catalyzed by the ternary Au-Ga-Se nanoparticles. The process is thermally activated: if the substrate temperature is too low, after nucleation as soon as the nanoparticle is depleted from Ga the growth stops, as demonstrated by the data in Fig. 1 and 2. The growth process can occur via the VLS or VSS mechanism depending on the Ga and Se content and its spatial distribution in the NPs (including the shell layer). Solidification of the NP may also be due to a low Ga concentration under insufficient Ga supply from the substrate. The presence of nearly spherical NPs instead of spherical cap, together with the kinks seldom observed in the NWs, as in Fig. 2(b) and Fig. 7(d), and the morphology of the worm-like nanostructures that grow when the nanoparticles are large, are suggestive of the morphology observed in ZsSe NWs grown by Au assisted VSS reported by Zannier et al. [35, 44]. However, our data do not presently allow for any definite conclusion on the VLS or VSS growth mode. This important question will be addressed elsewhere. It is clear, however, that Ga_2Se_3 forms by binding Ga and Se atoms in the NPs. The known formation enthalpies of the compounds of interest are −87.7 kJ/mol for GaAs [45], −159.0 kJ/mol for GaSe and [46], −405.9 kJ/mol for Ga_2Se_3 [46] (at room temperature), 5.58 kJ/mol for metallic Ga [47], -23.9 kJ/mol for AuGa (at 433°C) [47], and 24.8 kJ/mol for $AuGa_2$ (at 427°C) [47]. Therefore, Ga_2Se_3 is by far the most stable compound and crystallizes from the ternary Au-Ga-Se NPs regardless of their state (solid,

liquid or partially molten). Being Ga_2Se_3 more stable than the Au-Ga compounds, the growth of the Ga_2Se_3 nanostructure continuously depletes from Ga the Au agglomerates lying on the substrate, that therefore continue to trigger the GaAs decomposition, with the formation of voids and penetration of Au agglomerates deep in the substrate (see Fig. 11a).

Figure 3 shows that the NW length exhibit a strikingly nonmonotonic dependence on exposure time to the Se flux, with initially linear correlation, saturation at a maximum value, followed by shortening for longer exposure times. Out-of-plane NWs, catalyzed by the smallest Au nanoparticles always grow simultaneously with thicker in-plane worm-like structures, similarly to what was observed for the VSS-grown ZnSe NWs in Ref. [44]. We speculate that these in-plane structures effectively encapsulate the GaAs substrate [42] and/or stop the Ga diffusion flux to the NWs at a certain coverage thus stopping the growth.

According to the data in Fig. 2, higher Se fluxes yield smaller maximum NW lengths and shorter critical times after which the NWs start to shorten. The time necessary to cover the GaAs free surface with wormlike structures is shorter in case of higher Se flux, resulting in the stop of Ga feeding of NW growth at a shorter length.

As the Ga flux is stopped, we can imagine that the Se flux may induce the crystallization of a thin Ga_2Se_3 shell at the surface of the metal nanoparticle. A few nm thick shell is indeed observed in the TEM images as shown in Fig. 7(a). Due to the surface sensitivity of XPS, the presence of this shell, the penetration of the larger Au agglomerates deep in the substrate and the coverage of the GaAs surface with Ga_2Se_3 wormlike structures well justify the complete attenuation of XPS signal of both the Au 4f and As3d observed in Figs. 8 and 9.

The maximum NW length observed in the explored growth condition was 3 μm and was obtained in case of growth with low Se BEP. This could not be an intrinsic limit but the result of

the competition between in plane coverage of the surface and out of plane NW growth as described above. Backward diffusion of Ga from the NWs to the substrate surface may lead to the NW shortening in the late stage of growth.

We now try to understand more deeply the NW growth process within a diffusion transport model. In the absence of Ga deposition, growth should be limited by surface diffusion of Ga adatoms released from the GaAs substrate. The standard diffusion equation for Ga adatoms on the NW sidewalls [48] is then given by

$$D\frac{d^2n}{dz^2} = \frac{n}{\tau}, \;\; n(z=0) = n_s(t), \;\; n(z=L) = n_l. \qquad (1)$$

Here, z is the coordinate along the NW axis, L is the actual NW length (not to be confused with the projected length used elsewhere in this paper), $D$is the diffusion coefficient and τ is the effective lifetime of Ga adatoms [49]. The concentration n_s at the substrate surface may be time-dependent because the morphology and even material of the substrate surface (initially GaAs and then Ga_2Se_3) changes with the growth time t. In contrast, the concentration n_l at the liquid-solid interface is assumed independent of time under the stationary conditions. The axial NW growth rate is given by [48]

$$\frac{dL}{dt} = -\frac{\Omega}{R} D \left.\frac{\partial n}{\partial z}\right|_{z=L}. \qquad (2)$$

Here, Ω is the elementary volume of Ga_2Se_3 in the solid state and R is the NW radius. This growth rate is transport-limited and hence independent on whether the NP is liquid or solid.

From Eqs. (1) and (2), it is easy to obtain

$$\frac{dL}{dt} = \frac{\Omega}{\tau}\frac{\lambda}{R}\frac{[n_s(t)-n_l]}{tanh(L/\lambda)}, \qquad (3)$$

with $\lambda = \sqrt{D\tau}$ as the effective diffusion length of the Ga adatoms. This expression is similar to that previously obtained in Ref. [50], where the growth of CdTe NWs was controlled by a

diffusion flux of Te from the substrate in the absence of Te deposition. The NW length saturates at $L/\lambda >> 1$ when $n_s > n_l$, meaning that no further growth is possible when all adatoms are trapped on the sidewalls or re-evaporate from the surface, as observed in Ref. [45]. Clearly, the growth rate given by Eq. (3) is positive only if $n_s > n_l$, that is, when Ga adatoms on the substrate surface have a higher concentration than in the liquid droplet, and negative otherwise. The case of $n_s < n_l$ corresponds to the so-called negative growth [48], in which NWs shorten by evaporating excess Se atoms and transferring Ga atoms from the NP to the substrate along the sidewalls by surface diffusion.

According to Ref. [50], the diffusion length of Ga adatoms at the growth temperatures is larger than 2 μm (for GaAs NWs), while our Ga_2Se_3 NWs are typically shorter than 1 μm. Therefore, we can use the approximation of $L/\lambda << 1$, in which case integration of Eq. (3) gives

$$L = \sqrt{\frac{2\Omega D}{R}}\left\{\int_0^t dt'[n_s(t') - n_l]\right\}^{1/2}, \quad (4)$$

which does not contain λ. At a time-independent $n_s - n_l > 0$, this results in the diffusion-like growth law $L \propto (Dt/R)^{1/2}$ [51], showing that thinner NWs grow faster. The NW length scales as the square root of time and increases toward higher temperatures due to enhanced thermally activated diffusion ($L \propto D^{1/2}$). This qualitatively explains why our NWs grow only at elevated temperatures, as observed in Fig. 2. However, according to Fig. 3, the NW length first increases linearly with time and then decreases after a critical length has been reached.

This behavior is likely to be associated with a time-dependent concentration of Ga adatoms n_s in Eq. (4), which is initially higher than n_l to enable nucleation and growth of NWs, and then becomes lower than n_l to start the NW shortening by negative diffusion from the NP to the substrate. We assume that Ga adatoms are produced at the rate J_+ per unit time per unit area

of GaAs substrate exposed to the Se flux, and consumed by growing parasitic worm-like structures, which block surface diffusion of Ga to the NW tip. Progressive coverage of the surface by these parasitic structures is described by the simplest Kolmogorov model [52] in the form $1 - exp(-\omega t)$, with ω as the corresponding growth rate (1/min). These considerations yield

$$\frac{dn_s}{dt} = J_+ e^{-\omega t} - J_-(1 - e^{-\omega}), n_s(t = 0) = n_l. \quad (5)$$

The initial condition corresponds to equilibrium between the droplet and the substrate at $t = 0$, where no growth occurs. Solving this, we obtain the adatom concentration in the form

$$n_s(t) - n_l = \frac{(J_+ + J_-)}{\omega}(1 - e^{-\omega}) - J_- t, \quad (6)$$

showing that $n_s - n_l = J_+ t$ at $\omega t << 1$ and $n_s - n_l = (J_+ + J_-)/\omega - J_- t$ at $\omega t >> 1$. Hence, the force driving the surface diffusion increases linearly with time at the beginning of the growth, the GaAs substrate being still clean. Towards the end of the growth, it decreases due to nucleation and growth of the parasitic worm-like structures and finally becomes negative, which is why the NW lengths finally shorten.

Integrating Eq. (6) and using the result in Eq. (4), our final expression for the NW length is given

$$L = vt\left[-\alpha + 2\frac{2(1+\alpha)}{x} - \frac{2(1+\alpha)}{x^2}(1 - e^{-\omega t})\right]^{1/2}, \quad (7)$$

with $v = \sqrt{(\Omega D J_+)/R}$, $\alpha = J_-/J_+$, and $x = \omega t$. As expected, the linear growth law $L = vt$ always occurs at $\omega t << 1$. Figure 12 shows the fits to the mean NW lengths versus time under different Se fluxes, obtained from Eq. (7) with the parameters summarized in Table 2.

According to the model, the NW growth in the initial stage is controlled by the production rate of Ga adatoms released from the GaAs surface. This depends on the Se flux: the higher is the

latter, the faster is the GaAs decomposition providing Ga for nucleation and growth of Ga_2Se_3 NWs in the absence of Ga supply from vapor. The NW growth process is therefore limited by Ga transport, but its production rate is enhanced for higher Se input. The axial NW growth rate is therefore faster for higher Se fluxes. On the other hand, parasitic structures also emerge faster under higher Se fluxes, which explains why the NW lengths starts to decrease earlier.

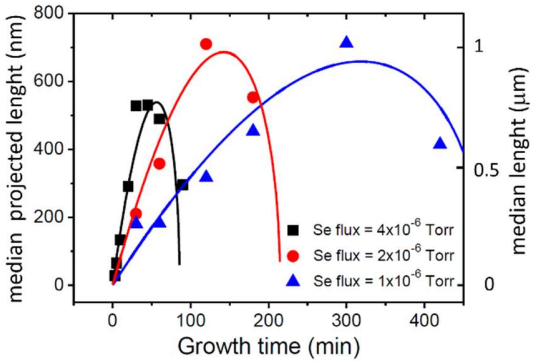

Figure 12. Evolution of the median length of Ga_2Se_3 NWs with time at the fixed temperature of 560ºC and for different Se fluxes (symbols from Fig. 3), fitted by Eq. (7) (lines) with the parameters summarized in Table 2. The elongation rate in the initial linear growth stage is increased for higher Se fluxes. On the other hand, parasitic structures also emerge faster on the rest of the surface, which is why the NWs length starts to decrease earlier at higher Se fluxes.

Table 2. Fitting parameters of Ga_2Se_3 NWs obtained from the fits in Fig. 12

Se BEP (Torr)	Linear elongation rate ν (nm/min)	Growth rate of surface coverage ω (1/min)	Critical coverage	Ratio J_+/J_-
4×10^{-6}	17	0.0058	0.25	5.8
2×10^{-6}	8.6	0.0017	0.24	7.8
1×10^{-6}	3.6	0.00037	0.15	16.7

This explains the very different slope angles of the linear parts of elongation rates in Table 1, decreasing from ~ 24 nm/min to ~ 5.3 nm/min as Se BEP decreases from 4×10^{-6} Torr to 1×10^{-6} Torr (these values are given for the actual NW lengths). On the other hand, the maximum NW length is limited by the growth of the parasitic worm-like structures, whose rate should also increase for higher Se fluxes. According to Table 2, the growth rate of the surface coverage decreases from ~ 0.0058 1/min at 4×10^{-6} Se BEP to ~ 0.00037 1/min at 1×10^{-6} Se BEP. It is interesting to note that the maximum NW length is reached at a critical fractional coverage of ~ 0.2 in all cases. Finally, the best fits to the data are obtained for the J_-/J_+ratio much larger than unity and increasing toward lower Se fluxes. Overall, both the NW growth process and the coverage of GaAs surface by the parasitic structures occur faster at higher Se fluxes. According to our data, the maximum NW lengths are reached at lower Se fluxes, but this requires much longer growth times (~ 300 min at a Se BEP of 1×10^{-6} Torr).

CONCLUSIONS

In conclusion, we have presented a set of experimental data showing how thin epitaxial Ga_2Se_3 NWs can be obtained on GaAs substrates in the absence of any external Ga supply by a heterovalent exchange reaction assisted by Au NPs. Thicker worm-like Ga_2Se_3 nanostructures are also found lying on the substrate surface. Both kinds of nanostructures display Au-rich NPs at the tip. Chemical and structural analysis of the NPs and NWs at different stages of growth demonstrated that the presence of Au NPs is essential for obtaining Ga_2Se_3 NWs by this method. It has been found that the NW elongation stops at a growth time that depends on the incoming Se flux. Further increase in time at the growth temperature leads to NW shortening at a rate which is

independent of the Se supply. This growth mechanism has been described within a diffusion transport model, which explains the nonmonotonic behavior of the NW length as due to the blocking of the Ga supply from the substrate when covered with parasitic worm-like structures and the ensuing negative diffusion of the Ga atoms from the NPs to the NW sidewalls. The growth of Ga_2Se_3 NWs has been demonstrated here for the first time to our knowledge and can work equally well in a wide range of epitaxy techniques.

ASSOCIATED CONTENT

Supporting Information. NW growth with and without Bismuth flux. Determination of the growth direction of the NWs. Influence of the Au NP diameter on the morphology of Ga_2Se_3 nanostructures. Diameter of the NWs versus growth time and Se BEP. Chemical composition of worm-like nanostructures**.** The following file is available free of charge.

Ga2Se3 SI.pdf

AUTHOR INFORMATION

Corresponding Author

*Silvia Rubini Istituto Officina dei Materiali, Consiglio Nazionale delle Ricerche, Trieste, Italy

orcid.org/0000-0001-5215-2223

+39 040 3756437

rubini@iom.cnr.it

Present Addresses

¥ Politecnico di Torino, Corso Duca degli Abruzzi, 24, 10129 Torino, Italy

† Department of Chemistry, Durham University, Lower Mountjoy, South Road, Durham DH1 3LE, UK

Author Contributions

The manuscript was written through contributions of all authors. All authors have given approval to the final version of the manuscript. ‡These authors contributed equally. (match statement to author names with a symbol)

ACKNOWLEDGMENT

VGD thanks the Russian Science Foundation for financial support under Grant No. 19-72-30004. For MF, KF and SG this work was financially supported from the Slovenian Research Agency, research core funding No. P2-0412. This work has been performed in the framework of the Nanoscience Foundry and Fine Analysis (NFFA-MIUR Italy Progetti Internazionali) project.

REFERENCES

[1] Ohta, T.; Schmidt, D. A.; Meng, S.; Klust, A.; Bostwick, A.; Yu, Q.; Olmstead, M. A.; Ohuchi, F. S. Intrinsic Vacancy-Induced Nanoscale Wire Structure in Heteroepitaxial Ga_2Se_3 /Si(001). *Phys. Rev. Lett.* **2005**, 94 (11), 1–4.

[2] Finkman, E.; Tauc, J.; Kershaw, R.; Wold, A. Lattice Dynamics of Tetrahedrally Bonded Semiconductors Containing Ordered Vacant Sites. *Phys. Rev. B* **1975**, 11 (10), 3785-3794.

[3] Lübbers, D.; Leute, V. The Crystal Structure of β-Ga_2Se_3. *J. Solid State Chem*. **1982**, 43 (3), 339–345.

[4] Wright, A.; Williams, J.; Krost, A.; Richter, W.; Zahn, D. High Resolution and Conventional Transmission Electron Microscopy of Ga_2Se_3 Thin Films Grown by Vapour Phase Epitaxy. *J. Cryst. Growth* **1992**, 121, 111–120.

[5] Peressi, M.; Baldereschi, A. Structural and Electronic Properties of Ga_2Se_3. *J. Appl. Phys.* **1998**, 83 (6), 3092–3095.

[6] Ueno, K.; Kawayama, M.; Dai, Z. R.; Koma, A.; Ohuchi, F. S. Growth and Characterization of GaSe/GaAs (100) Epitaxial Thin Films. *J. Cryst. Growth* **1999**, 207, 69–76.

[7] Ueno, K.; Tokuchi, S.; Saiki, K.; Koma, A. Epitaxial Growth of a Vacancy-Ordered Ga_2Se_3 Thin Film on a Vicinal Si (001) Substrate. *J. Cryst. Growth* **2002**, 239, 1610–1614.

[8] Menke, D. R.; Qiu, J.; Gunshor, R. L.; Kobayashi, M.; Li, D.; Nakamura, Y.; Otsuka, N. An X-Ray Photoelectron Spectroscopy Study of Bonding at II-VI/III-V Heterovalent Interfaces. *J. Vac. Sci. Technol. B Microelectron. Nanom. Struct*. **1991**, 9 (4), 2171–2175.

[9] Krost, A.; Richter, W.; Zahn, D. R. T.; Brafman, O. Compound Formation and Large Microstrains at the Interface of 11-VI / III-V Semiconductors Detected by Raman Spectroscopy. *Semicond. Sci. Technol*. **1991**, 6, A109–A114.

[10] Kolodziejczyk, M.; Filz, T.; Krost, A.; Richter, W.; Zahn, D. R. T. The Likelihood of III_2-VI_3 compound Formation during Epitaxial Growth of II-VI on III-V Semiconductors. *J. Cryst. Growth* **1992**, 117 (1–4), 549–553.

[11] Okamoto, T.; Kojima, N.; Yamada, A.; Konagai, M.; Takahashi, K.; Nakamura, Y.; Nittono, O. Optical Anisotropy of Vacancy-Ordered Ga_2Se_3 Grown by Molecular Beam Epitaxy. *Jpn. J. Appl. Phys*. **1992**, 31 (2), 143–144.

[12] Okamoto, T.; Konagai, M.; Kojima, N.; Yamada, A.; Takahashi, K.; Nakamura, Y.; Nittono, O. Anomalous Anisotropy in the Absorption Coefficient of Vacancy-Ordered Ga_2Se_3. *J. Electron. Mater.* **1993**, 22 (2), 229–232.

[13] Okamoto, T.; Yamada, A.; Konagai, M.; Takahashi, K. Polarized Photoluminescence in Vacancy-Ordered Ga_2Se_3. *J. Cryst. Growth* **1994**, 138 (1–4), 204–207.

[14] Ding, J.; Zhou, Y.; Cui, Y.; Fu, Z. Ga 2 Se 3 Thin Film as a Negative Electrode Material for Lithium-Ion Batteries. *ECS Electrochem. Lett*. **2012**, 1 (1), 7–9.

[15] Jin, H.; Zhang, H.; Li, J.; Wang, T.; Wan, L.; Guo, H.; Wei, Y.; Zhang, H.; Li, J.; Wang, T.; Wan, L.; Guo, H.; Wei, Y. Data-Driven Systematic Search of Promising Photocatalysts for Water Splitting under Visible Light. *J. Phys. Chem. Lett*. **2019**, 10, 5211–5218.

[16] Yitamben, E. N.; Lovejoy, T. C.; Pakhomov, A. B.; Heald, S. M.; Negusse, E.; Arena, D.; Ohuchi, F. S.; Olmstead, M. A. Correlation between Morphology, Chemical Environment, and Ferromagnetism in the Intrinsic-Vacancy Dilute Magnetic Semiconductor Cr-Doped Ga_2Se_3/Si(001). *Phys. Rev. B - Condens. Matter Mater. Phys*. **2011**, 83 (4), 1–9.

[17] Li, D.; Nakamura, Y.; Otsuka, N.; Qiu, J.; Kobayashi, M.; Gunshor, R. L. Reconstruction at the Ga_2Se_3/GaAs Epitaxial Interface. *J. Vac. Sci. Technol. B Microelectron. Nanom. Struct*. **1991**, 9 (4), 2167–2170.

[18] Teraguchi, N.; Kato, F.; Konagai, M.; Takahashi, K.; Nakamura, Y.; Kato, F.; Konagai, M.; Takahashi, K. Vacancy Ordering of Ga_2Se_3 Films by Molecular Beam Epitaxy of GaP Films by Molecular Beam Epitaxy. *Appl. Phys. Lett*. **1991**, 59, 567–569.

[19] Zahn, D. R. T.; Krost, A.; Kolodziejczyk, M.; Richter, W. Epitaxial Ga_2Se_3 Layers Grown on GaAs(100) Using a Heterovalent Exchange Reaction. *J. Vac. Sci. Technol. B Microelectron. Nanom. Struct*. **1992**, 10 (4), 2077.

[20] Li, B.; Xia, Y.; Ho, W.; Xie, M. Suspended Ga_2Se_3 Film and Epitaxial Bi_2Se_3 (221) on GaSb (001) by Molecular-Beam Epitaxy. *J. Cryst. Growth* **2017**, 459, 76–80.

[21] Safdar, M.; Wang, Z.; Mirza, M.; Jiang, C.; He, J. Crystalline Indium Sesquitelluride Nanostructures: Synthesis, Growth Mechanism and Properties. *J. Mater. Chem.* **2012**, *22* (36), 19228–19235.

[22] Wang, Z.; Safdar, M.; Jiang, C.; He, J. High-Performance UV-Visible-NIR Broad Spectral Photodetectors Based on One-Dimensional In 2Te 3 Nanostructures. *Nano Lett.* **2012**, *12* (9), 4715–4721.

[23] Hsin, C. L.; Huang, C. W.; Wu, M. H.; Cheng, S. Y.; Pan, R. C. Synthesis and Thermoelectric Properties of Indium Telluride Nanowires. *Mater. Res. Bull.* **2019**, *112* (November 2018), 61–65.

[24] Sun, X.; Yu, B.; Ng, G.; Nguyen, T. D.; Meyyappan, M. III-VI Compound Semiconductor Indium Selenide (In_2Se_3) Nanowires: Synthesis and Characterization. *Appl. Phys. Lett.* **2006**, 89 (23), 1–4.

[25] Bartolomé, J.; Maestre, D.; Cremades, A. Synthesis of In2S3 and In6S7 Microcolumns and Nanowires by a Vapor-Solid Method. *Phys. Status Solidi Appl. Mater. Sci.* **2018**, *215* (19), 1–7.

[26] Peng, H.; Schoen, D. T.; Meister, S.; Zhang, X. F.; Cui, Y. Synthesis and Phase Transformation of In_2Se_3 and $CuInSe_2$ Nanowires. *J. Am. Chem. Society* **2007**, 3, 6–9.

[27] Zhai, T.; Fang, X.; Liao, M.; Xu, X.; Liang, L.; Badoan, L.; Koide, Y.; Ma, Y.; Yao, Y.; Bando, Y.; Goldberg, D. Fabrication of High-Quality In_2Se_3 Nanowire Arrays toward High-Performance Visible-Light Photodetectors. *ACS Nano* **2010**, 4 (3), 1596–1602.

[28] Suryawanshi, S. R.; Bankar, P. K.; More, M. A.; Late, D. J. Vapour-Liquid-Solid Growth of One-Dimensional In2Se3 Nanostructures and Their Promising Field Emission Behaviour. *RSC Adv.* **2015,** 5 (80), 65274–65282.

[29] Peng, H.; Zhang, X. F.; Twesten, R. D.; Cui, Y. Vacancy Ordering and Lithium Insertion in III_2VI_3 Nanowires. *Nano Res.* **2009**, 2 (4), 327–335.

[30] Chan, C.K.; Peng, H.; Liu, G.; McIlwrath, K.; Zhang, X.F.; Huggins, R.A. High-performance lithium battery anodes using silicon nanowires. *Nature Nanotechnology* **2007**, 3, 31-35.

[31] Wang, L.; Tu, C. Growth Modulation of Ga_2S_3 Horizontal Nanowires and Its Optical Properties. *Nanotechnology* **2020**, 31 (16), 165603.

[32] Sutter, E.; French, J. S.; Balgarkashi, A.; Tappy, N.; Fontcuberta I Morral, A.; Idrobo, J. C.; Sutter, P. Single-Crystalline γ-Ga_2S_3 Nanotubes via Epitaxial Conversion of GaAs Nanowires. *Nano Lett.* **2019**, 19 (12), 8903–8910.

[33] Begum, N.; Bhatti, A. S.; Jabeen, F.; Rubini, S.; Martelli, F. Lineshape Analysis of Raman Scattering from LO and so Phonons in III-V Nanowires. *J. Appl. Phys*. **2009**, 106 (11), 114317.

[34] M. Ek, M; Lehmann, S; Wallenberg, L. R. Electron channelling: challenges and opportunities for compositional analysis of nanowires by TEM. 2020 *Nanotechnology* in press, https://doi.org/10.1088/1361-6528/ab9679.

[35] Zannier, V.; Grillo, V.; Martelli, F.; Plaisier, J. R.; Lausi, A.; Rubini, S. Tuning the Growth Mode of Nanowires via the Interaction among Seeds, Substrates and Beam Fluxes. *Nanoscale* **2014**, 6 (14), 8392–8399.

[31] Petro, W. G.; Kendelewicz, T.; Lindau, I.; Spicer, W. E. Au-GaAs(110) Interface: Photoemission Studies of the Effects of Temperature. *Phys. Rev. B* **1986**, 34 (10), 7089–7106.

[32] Lindau, I.; Pianetta, P.; Yu, K. Y.; Spicer, W. E. Photoemission of Gold in the Energy Range 30-300 EV Using Synchrotron Radiation. *Phys. Rev. B* **1976**, 13 (2), 492–495.

[33] Kraut, E. A.; Grant, R. W.; Waldrop, J. R.; Kowalczyk, S. P. Semiconductor Core-Level to Valence-Band Maximum Binding-Energy Differences: Precise Determination by x-Ray Photoelectron Spectroscopy. *Phys. Rev. B* **1983**, 28 (4), 1965–1977.

[34] Surdu-Bob, C. C.; Saied, S. O.; Sullivan, J. L. An X-Ray Photoelectron Spectroscopy Study of the Oxides of GaAs. *Appl. Surf. Sci*. **2001**, 183, 126–136.

[35] Dao, K. A.; Phan, A. T.; Do, H. M.; Luu, T. H.; Falke, M.; MacKenzie, M. The Influences of Technological Conditions and Au Cluster Islands on Morphology of Ga_2O_3 Nanowires Grown by VLS Method on GaAs Substrate. *J. Mater. Sci. Mater. Electron*. **2011**, 22 (2), 204–216.

[36] Dao, K. A.; Nguyen, T. D.; Phan, A. T.; Do, H. M. On the Formation of Voids, Etched Holes, and GaO Particles Configuration during the Nanowires Growth by VLS Method on GaAs Substrate. *J. Mater. Sci. Mater. Electron*. **2013**, 24 (7), 2513–2520.

[37] Barcz, A. J.; Piotrowska, A. Fundamental and practical aspects of alloying encapsulated gold-based contacts to GaAs. *Thin Solid Films* **1987**, 149, 251–260.

[38] Mojzes, I.; Sebestyen, T.; Szigethy, D. Volatile component loss and contact resistance of metals on GaAs and GaP during annealing. *Solid. State. Electron*. **1982**, 25 (6), 449–460.

[39] Katsunori, Y.; Takeda, Y.; Kameda, K.; Itagaki, K. Measurements of Heat of Formation of GaP, InP, GaAs, InAs,GaSb and InSb. *Materials Transactions, JIM* **1994**, 35(9) 596–602.

[40] Ider, M.; Pankajavalli, R.; Zhuang, W.; Shen, J. Y.; Anderson, T. J. Thermochemistry of the Ga-Se System. *ECS J. Solid State Sci. Technol*. **2015**, 4 (5), Q51.

[41] Predel, B.; Stein, D. W. Bildungsenthalpien Binaerer Verbindungen Des Gallium Mit Kupfer, Silber Und Gold Sowie Analyse de Thermodynamischen Eigenschaften von 3/2-Electronen-Verbindungen. *Acta Metall.* **1972**, 20, 681–692.

[42] Zannier, V.; Grillo, V.; Rubini, S. Diameter-Dependent Morphology of Vapour-Solid-Solid Grown ZnSe Nanowires. *J. Phys. D. Appl. Phys*. **2014**, 47, 394005.

[43] Dubrovskii.;. Sibirev N. V.; Cirlin.; Bouravleuv A. D.; Samsonenko Yu. B.; Dheeraj D. L.; Zhou H. L.; Sartel C.; Harmand.; Patriarche G.; Glas F. Role of non-linear effects in nanowire growth and crystal phase, *Phys. Rev. B* **2009**, 80, 205305.

[44] Dubrovskii V. G. *Nucleation theory and growth of nanostructures*. Springer, Heidelberg – New York – Dordrecht – London, 2014.

[45] Di Carlo, V.; Prete, P.; Dubrovskii, V. G.; Berdnikov, Y.; Lovergine, N. CdTe Nanowires by Au-Catalyzed Metalorganic Vapor Phase Epitaxy. *Nano Lett*. **2017**, 17 (7), 4075–4082.

[46] Harmand, J. C.; Glas, F.; Patriarche, G. Growth Kinetics of a Single $InP_{1-X}As_x$ Nanowire. *Phys. Rev. B - Condens. Matter Mater. Phys*. **2010**, 81 (23), 1–8.

[47] Dubrovskii, V. G.; Xu, T.; Lambert, Y.; Nys, J. P.; Grandidier, B.; Stiévenard, D.; Chen, W.; Pareige, P. Narrowing the Length Distribution of Ge Nanowires. *Phys. Rev. Lett.* **2012**, 108 (10), 1–5.

[48] Dubrovskii, V. G. Nucleation and growth of adsorbed layer: self-consistent approach based on Kolmogorov-Avrami model, *Phys. Stat. Sol. (b)* **1992**, 171, 345-356.

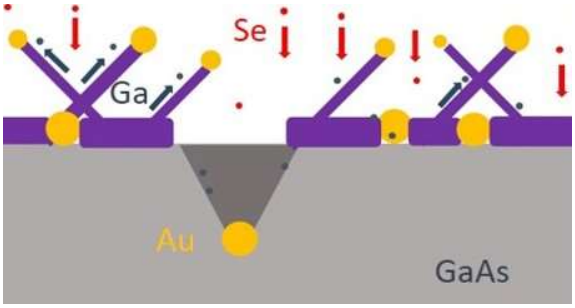
Se
Ga
Au
GaAs